ADMM-based Multiperiod Optimal Power Flow Considering Plug-in Electric Vehicles Charging

Hua Fan, Chao Duan, *Student Member, IEEE,* Chuan-Ke Zhang, *Member, IEEE,* L. Jiang, *Member, IEEE,* Chengxiong Mao, *Senior Member, IEEE,* and Dan Wang, *Senior Member, IEEE*

***Abstract*—When plug-in electric vehicles (PEVs) participate in grid operation, the inter-temporal feature of PEVs charging transforms the traditional optimal power flow (OPF) problem into multiperiod OPF (MOPF) problem. In the case that the population of PEVs is huge, the large number of variables and constraints render the centralized solution technique unsuitable to solve the MOPF problem. Therefore, a distributed algorithm based on alternating direction method of multipliers (ADMM) is developed to decompose the MOPF into two update steps that are solved in an alternating and iterative style. To improve the solution efficiency, the second update step is transformed into a Euclidean projection problem by approximating the original objective with a surrogate function. Then a projection algorithm is utilized to solve the approximate problem. Numerical results show that this reformulated model obtains suboptimal solutions with small relative error, but gains considerable speed-up. Furthermore, its scalability and effectiveness are tested in the 119-bus and 906-bus distribution networks.**

***Index Terms*—Plug-in electric vehicles, multiperiod optimal power flow, alternating direction method of multipliers (ADMM), projection algorithm.**

I. Introduction

WITH the proliferation of plug-in electric vehicles (PEVs), the optimal power flow (OPF) problem that considers the impacts of PEVs has been one of the crucial issues in power system operation. OPF aims to optimize a certain objective, such as generation cost or consumer utility. As a sort of controllable loads, PEVs can be used to fill load valleys or accommodate intermittent renewable generation. The majority of PEVs are charged in low-voltage distribution networks which usually have a tree topology.

AC OPF is generally nonconvex due to nonlinearity of power balance equations and global optimal solution cannot be guaranteed. Facing this challenge, various approaches of approximation or convex relaxation have been developed over the decades, such as direct current (DC) approximation [1], [2], semi-definite programming (SDP) relaxation [3]–[5], second-order cone (SOC) relaxation [6]–[8] and moment-based relaxations [9]–[12]. The SOC and SDP relaxation methods have respective advantages and disadvantages, thus many researchers try to combine them to achieve better solution performance than each of them. For instance, in [13], a quadratic convex (QC) relaxation is proposed and the case studies show that QC relaxation has better accuracy over the SOC relaxation and significantly faster computational speed than the SDP relaxation. In [14], a moment relaxation method that mixes SDP and SOC formulations is developed to substantially improve the computational speed. Essentially, some of the methods are equivalent under some conditions, e.g., SDP relaxation and SOC relaxation are equivalent and exact for radial networks [15] under some assumptions. See [16] for an overview of the equivalence relations among the relaxation methods. In practice, almost all the proposed methods can obtain zero-duality-gap solution unless some certain conditions are satisfied [3], [17]. In [18], the author proposes a method that selects an objective function based on a weighted Laplacian matrix and constrains the generation cost within a small range around the lower bound obtained from SDP relaxation. This method is able to find near globally optimal solutions to OPF problems. In some test systems, the SDP relaxations are observed to obtain the exact global optimums. But, in general, convex relaxation approaches produce an infeasible solution possibly close to the global optimum. The wide application of convex PF models are mainly due to the maturity of convex optimization solvers, e.g. sedumi, sdpt3 and mosek etc., which can efficiently solve convex problems of reasonably large scale. On the other hand, before the emergence of convex relaxation approaches, interior point method (IPM) had been a standard approach to solve OPF to local optimality and are applied to practical large-scale systems [19]–[21]. In some cases, the local solutions obtained by IPM actually coincide with the global optimums [13], [22]. From a practitioner's viewpoint, a feasible local solution is much more favorable than an infeasible solution even if it is close to the global optimum, i.e. the feasibility is prior to the optimality. Therefore, this paper directly employs the original AC power flow model without resorting to any convex relaxations.

The classical OPF problem optimizes the objective function in a single time period, while for a distribution network that incorporates PEVs, the inter-temporal constraints of the energy storage of PEVs makes it necessary to solve multiple OPF

This work is supported partially by the National Natural Science Foundation of China under Grant No. 51361130151 and by the Engineering and Physical Sciences Research Council under Grant EP/L001004/01. *(Corresponding author: Dan Wang.)*

H. Fan, C. Mao and D. Wang are with the State Key Laboratory of Advanced Electromagnetic Engineering and Technology, School of Electrical and Electronic Engineering, Huazhong University of Science and Technology, Wuhan 430074, China. (fanhua@hust.edu.cn, cxmao@hust.edu.cn, wangdan@mail.hust.edu.cn)

C. Duan is with the Department of Electrical Engineering, Xian Jiaotong University, Xian 710049, China, and also with the Department of Electrical Engineering and Electronics, University of Liverpool, Liverpool L69 3GJ, U.K. (e-mail: duanchao@stu.xjtu.edu.cn)

C.-K. Zhang is with the School of Automation, China University of Geosciences, Wuhan 430074, China (ckzhang@cug.edu.cn)

L. Jiang is with the Department of Electrical Engineering & Electronics, University of Liverpool, Liverpool, L69 3GJ, U.K. (ljiang@liv.ac.uk)

problems over a finite horizon, which is called multiperiod OPF (MOPF) [23]. Reference [24] develops a DC MOPF model that integrates energy storage and renewable energy sources. The authors in [25] propose a rolling MOPF model that schedules PEVs in a three-phase unbalanced distribution network. Due to the nonconvexity in the AC power flow equations, the convex relaxation method in single-period OPF can be extended to MOPF as well. For example, Jabr utilizes SOC relaxation to convexify the AC MOPF problem in [26], and the work in [27] solves the MOPF using a parallel moment approach.

According to the 2009 National Household Travel Survey (NHTS) [28], commuting to and from work begins predominately between 6:00 and 9:00 and between 16:00 and 18:00. Without loss of generality, we assume that PEV drivers charge their cars upon the last arrival at home. Thus PEVs charging would potentially add new peaks to conventional loads and exert negative impacts on a distribution network [29], such as increasing power losses or loading of lines and transformers. In recent years, various strategies of PEVs charging dispatch have been developed. Gan [30] proposes a decentralized algorithm that schedules PEV charging to fill the load valley. In [31], a smart distribution power flow framework and multiple charging strategies are proposed to overcome the drawbacks of uncontrolled charging that could increase the peak demand and lower nodal voltage. In [25], an optimal charging algorithm is developed to minimize the cost of PEVs charging in a three-phase unbalanced distribution network. However, this optimization method cannot apply in the case where the number of PEVs is huge. The authors of [32] develop a bi-level programming scheme to schedule PEVs while satisfying the network constraints. Although the numerical studies verify the convergence of this algorithm, there is no theoretical guarantee to confirm it. Indeed, the value of penalty coefficient significantly affects the optimal value and computing performance, hence it should be prudent to select the value.

In this paper, a hierarchical control scheme similar to the bi-level structure in [32] is adopted. Briefly speaking, the PEVs in a certain area are taken as an entity and controlled by an agent, generally termed as *aggregator*, which collects and dispatches the aggregate information of all the PEVs. PEV aggregator plays as a middleware between the fleet of electric vehicles and the distribution system operator (DSO) who is responsible for the optimal power flow calculation. To optimally schedule PEVs charging under this scheme, we develop an optimization model that combines branch flow model (BFM) and Alternating Direction Method of Multipliers (ADMM) due to two reasons: 1) BFM was first proposed in [33], [34] and proved to be suitable to model radial distribution networks; 2) Since ADMM is a variant of the augmented Lagrangian method, the optimal value can be achieved to a prespecified accuracy within a few of iterations.

The contributions of our work are as follows. The ADMM is used to accelerate the the PEVs charging scheduling problem. Besides, a projection model is developed to approximate the second update step in ADMM and solution of this model is easy to be carried out in parallel by the local controller of each PEV, which produces decent improvement in computational performance. As compared to the bi-level decomposition method in [32], our method can converge to the optimal objective value in less time, showing superior computation performance. Especially, the proposed ADMM-based approach can be scalable in large-scale scenarios, i.e., the size of distribution network or the number of PEVs is large.

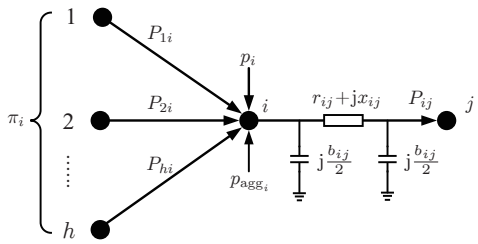

Fig. 1. Branch flow model.

The remainder of the paper is organized as follows. Section II formulates the mathematical model of MOPF that accounts for the constraints of a distribution network and of PEVs charging. Section III presents the MOPF based on ADMM, and finds an approximate model to solve the aggregator charging minimization step by using a projection model. Section IV verifies the accuracy of the proposed approximate model and validates its scalability in a large case. The conclusions are drawn in Section V.

II. Mathematical Formulation of Multiperiod OPF considering PEVs Charging

In this section, we construct the MOPF model that integrates PEVs in a distribution network. Both the constraints of network and the constraints of PEVs charging process are taken into consideration.

A. Constraints of Distribution Network

Without loss of generality, consider a radial distribution network that is represented by a directed graph $G = (\mathcal{N}, \mathcal{L})$. Denote the substation bus as 0 and other buses as $1, \ldots, N$. Let $\mathcal{N} := \{0, \ldots, N\}$ represent the set of all buses and let $p_i(t)$ and $q_i(t)$ denote the active and reactive power injection at this bus, respectively. As shown in Fig. 1, the branch is represented as π equivalent model. Each ordered pair (i, j) in $\mathcal{L}$ represents a line with series impedance $r_{ij} + \mathrm{j}x_{ij}$ and total charging susceptance b_{ij}, thus let $P_{ij}(t)$ and $Q_{ij}(t)$ denote denote the active and reactive power on the line from bus i to j, respectively. Let $\mathcal{T} := \{1, \ldots, T\}$ denote the set of time slots.

For each bus $i \in \mathcal{N}$ at time $t \in \mathcal{T}$, the power balance equations are given by

$$P_{ij}(t) = p_i(t) - P_{\mathrm{agg}_i}(t) + \sum_{h \in \pi_i} \big(P_{hi}(t) - r_{hi}\ell_{hi}(t)\big) \quad (1)$$

$$Q_{ij}(t) = q_i(t) + \sum_{h \in \pi_i} \big(Q_{hi}(t) - x_{hi}\ell_{hi}(t)\big) \quad (2)$$

where π_i denotes the collections of child buses of bus i, $P_{\mathrm{agg}_i}(t)$ he charging power of the aggregator connected to bus i, and $\ell_{ij}(t)$ is the square of current magnitude defined as

$$\ell_{ij}(t) = \frac{P_{ij}^2(t) + Q_{ij}^2(t)}{v_i(t)}. \tag{3}$$

The equations for the substation bus are slightly different from Eqs. (1) and (2) as follows

$$0 = p_0(t) - P_{\mathrm{agg}_0}(t) + \sum_{h\in\pi_0} \big(P_{h0}(t) - r_{h0}\ell_{h0}(t)\big) \tag{4}$$

$$0 = q_0(t) + \sum_{h\in\pi_0} \big(Q_{h0}(t) - x_{h0}\ell_{h0}(t)\big). \tag{5}$$

The equations of power flow on all lines $(i,j) \in \mathcal{L}$ are expressed as

$$\begin{aligned} v_i(t) - v_j(t) = {} & 2\big(r_{ij}P_{ij}(t) + x_{ij}Q_{ij}(t)\big) \\ & - (r_{ij}^2 + x_{ij}^2)\ell_{ij}(t),\ \forall t \in \mathcal{T} \end{aligned} \tag{6}$$

where $v_i(t)$ denotes the square of voltage magnitude at bus i.

The voltage magnitude limits are given by

$$v_i^{\min} \le v_i(t) \le v_i^{\max}, \quad \forall i \in \mathcal{N},\ \forall t \in \mathcal{T}. \tag{7}$$

It is stated in [35] that the ampacity constraint of the lines' current should take into account the current that flows in the charging susceptance of the line. The line ampacity limit for line $(i,j) \in \mathcal{L}$ at time $t \in \mathcal{T}$ is represented as

$$\ell_{ij}(t) + \frac{1}{4}b_{ij}^2 v_i(t) + b_{ij}Q_{ij}(t) \le \ell_{ij}^{\max}, \tag{8}$$

$$\ell_{ij}(t) + \frac{1}{4}b_{ij}^2 v_j(t) + b_{ij}\left(x_{ij}\ell_{ij}(t) - Q_{ij}(t)\right) \le \ell_{ij}^{\max}. \tag{9}$$

For simplicity of notion, we define the feasible set of network constraints by

$$\mathcal{F}_N := \Big\{P_{\mathrm{agg}_i}(t)\text{: (1)-(8)} \quad \forall i \in \mathcal{N}, t \in \mathcal{T}\Big\}. \tag{10}$$

B. Constraints of PEVs Charging

In the present framework of smart charging of PEVs, the aggregator plays a role of connecting the DSO and the PEVs and transmitting control signals between them. The information related to the PEVs is uploaded to the aggregator, including the SOC of batteries, the arrival and departure time and the battery capacity. The power of aggregator i equals the sum of charging power of all PEVs that are managed by the aggregator, i.e.,

$$P_{\mathrm{agg}_i}(t) = \sum_{n=1}^{M_i} P_{V_{i,n}}(t), \quad \forall t \in \mathcal{T} \tag{11}$$

where M_i denotes the number of PEVs controlled by the aggregator connected to bus i, and $P_{V_{i,n}}$ is the charging power of PEV n.

During each charging interval, the state of charge (SOC) of PEV k in the next period is provided by

$$\mathrm{SOC}_n(t) = \mathrm{SOC}_n(t-1) + \frac{\eta P_{V_{i,n}}(t)\Delta t}{C_{\mathrm{b},n}}, \quad t \in \mathcal{T} \tag{12}$$

where η is the charging efficiency, $C_{\mathrm{b},n}$ is the battery capacity, Δt is the time interval and $\mathrm{SOC}_n(0)$ denotes the initial SOC when charging begins. In the framework of PEV smart charing, we assume that the SOCs of PEVs can be accurately estimated by the battery management system [36], [37] and then uploaded to the PEV aggregator by the communication interface.

The diversity of PEV drivers' behaviors leads to a variety of charging profiles. Only during the time when a vehicle is connected to grid can it get charged at any rate from 0 to the maximum value, denoted $P_{V_{i,n}}^{\max}$, otherwise charging power is set to zero. The constraint of charging power is defined as

$$0 \le P_{V_n}(t) \le b_n(t), \quad \forall t \in \mathcal{T} \tag{13}$$

where $t_{\mathrm{a},n}$ and $t_{\mathrm{d},n}$ are respectively the arrival time and departure time of PEV n, and

$$b_n(t) = \begin{cases} 0, & t \notin [t_{\mathrm{a},n}, t_{\mathrm{d},n}] \\ P_{V_{i,n}}^{\max}, & t \in [t_{\mathrm{a},n}, t_{\mathrm{d},n}]. \end{cases} \tag{14}$$

Additionally, PEVs must not be overcharged in order to prolong the lifetime of batteries. Thus the SOCs are controlled in such a prespecified range

$$\mathrm{SOC}_n^{\min} \le \mathrm{SOC}_n(t) \le \mathrm{SOC}_n^{\max}, \quad \forall t \in \mathcal{T}. \tag{15}$$

Similarly, the feasible set of constraints for PEVs charging is given by

$$\begin{aligned} \mathcal{F}_V := \Big\{ & P_{V_{i,n}}(t)\text{: (12)-(15)} \\ & \forall i \in \mathcal{N}, t \in \mathcal{T}, n = \{1, \ldots, M_i\}\Big\}. \end{aligned} \tag{16}$$

Thus, $\mathcal{F}_N$ and $\mathcal{F}_V$ are coupled through constraint (11).

C. Objective Function

In the context of economic dispatch of distribution network, minimization of energy losses is often used to reduce the cost [38]. The overall energy losses are represented as

$$E_{\mathrm{loss}} = E_{\mathrm{sub}} - E_{\mathrm{load}} - E_{\mathrm{EV}},$$

where E_{sub} denotes the overall energy absorbed from the substation, E_{load} the energy of basic loads excluding the PEVs and E_{EV} the overall energy charged by PEVs. In this paper, we assume that the initial and expected SOCs of each PEV are known *a priori*, therefore the value of E_{EV} are constant during the scheduling horizon $\mathcal{T}$. Besides, we also assume the basic loads (E_{load}) can be accurately forecasted and thus can be regarded as deterministic. Consequently, the optimization objective is equivalent to minimizing the overall energy absorbed from the substation, *i.e.*,

$$f_{\mathrm{obj}} = \sum_{t\in\mathcal{T}} p_0(t)\Delta t \tag{17}$$

where Δt denotes the time interval.

Although the distributed generation (DG) is not quite pervasive at present, it is developing rapidly and a promising trend of future power grid. When DGs, such as rooftop PVs, are integrated in distribution networks, the values of generation can be simply treated as forecasted power injections at certain nodes. Further consideration of the uncertainties of the DGs

is out of the scope of this paper and can be solved in the following work.

To summarize, the MOPF problem can be formulated in a more compact form as follows

$$\begin{aligned} \min \quad & f_{\text{obj}} \\ \text{s.t.} \quad & P_{\text{agg}_i}(t) \in \mathcal{F}_N,\ P_{V_{i,n}}(t) \in \mathcal{F}_P \\ & \text{Equation (11).} \end{aligned} \tag{18}$$

III. Formulation of Multiperiod OPF Problem based on ADMM

When the population of PEVs is large, the number of variables and constraints becomes huge, thus making it difficult to solve the multiperiod OPF problem. As can be observed in Section II, the constraints of the network and PEVs are only coupled through the aggregator. Therefore, In this paper we adopt ADMM to decouple the constraints to relieve the computation burden. In this section, we first give an illustrative introduction to the ADMM and then apply it to decompose the MOPF problem into two separable parts.

A. ADMM

ADMM is an algorithm that takes advantage of both the decomposability of dual ascent and the superior convergence properties of the method of multipliers [39]. This method solves problems in such form

$$\begin{aligned} \min \quad & f(x) + g(z) \\ \text{s.t.} \quad & Ax + Bz = c, \end{aligned} \tag{19}$$

with optimization variables $x \in \mathbb{R}^n$ and $z \in \mathbb{R}^m$, where $A \in \mathbb{R}^{p\times n}$, $B \in \mathbb{R}^{p\times m}$, and $c \in \mathbb{R}^p$ are known parameters.

Under the framework of ADMM, x and z are solved in an alternating fashion, *i.e.*, in each iteration x is first solved with z fixed and then z is solved with x fixed as the value obtained in the previous step. The iterates are carried out as the following procedures (see [39] and the references therein for more details):

$$\begin{aligned} x^{k+1} &:= \underset{x}{\text{argmin}}\left\{ f(x) + \frac{\rho}{2}\|Ax + Bz^k - c + u^k\|_2^2 \right\} \\ z^{k+1} &:= \underset{z}{\text{argmin}}\left\{ g(z) + \frac{\rho}{2}\|Ax^{k+1} + Bz - c + u^k\|_2^2 \right\} \\ u^{k+1} &:= u^k + Ax^{k+1} + Bz^{k+1} - c, \end{aligned} \tag{20}$$

where $\rho > 0$ is the penalty parameter and u is a vector of the Lagrangian multipliers. In order to certify the convergence of iterates, we define the stopping conditions by

$$\begin{aligned} \|Ax^k + Bz^k - c\|_2 &\le \epsilon^{\text{prim}} \\ \|\rho A^T B(z^{k+1} - z^k)\|_2 &\le \epsilon^{\text{dual}}, \end{aligned} \tag{21}$$

where ϵ^{prim} and ϵ^{dual} are tolerance parameters that are pre-specified in terms of expected accuracy. If the criteria hold, then we can claim that problem (19) is solved to optimality.

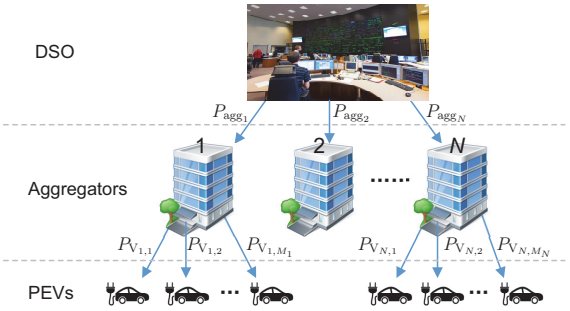

Fig. 2. The communication structure of the ADMM-based MOPF solution.

B. ADMM-based MOPF

By applying the ADMM, the iterative solution procedures of the MOPF can be formulated as follows:

$$\begin{aligned} \mathbf{P}_{\text{agg}_i}^{k+1} := \underset{\mathbf{P}_{\text{agg}_i}}{\text{argmin}} \Bigg\{ & f_{\text{obj}} + \mathbb{I}_N \\ & + \frac{\rho}{2}\sum_{i\in\mathcal{N}} \left\| \mathbf{P}_{\text{agg}_i} - \mathbf{1}^\intercal \mathbf{P}_{V_i}^k + u^k \right\|_2^2 \Bigg\} \end{aligned} \tag{22}$$

$$\mathbf{P}_{V_i}^{k+1} := \underset{\mathbf{P}_{V_i}}{\text{argmin}} \left\{ \mathbb{I}_{V_i} + \frac{\rho}{2}\left\| \mathbf{P}_{\text{agg}_i}^{k+1} - \mathbf{1}^\intercal \mathbf{P}_{V_i} + u^k \right\|_2^2 \right\} \tag{23}$$

$$u^{k+1} := u^k + \sum_{i\in\mathcal{N}} \left(\mathbf{P}_{\text{agg}_i}^{k+1} - \mathbf{1}^\intercal \mathbf{P}_{V_i}^{k+1} \right), \tag{24}$$

where $\mathbf{P}_{\text{agg}_i} \in \mathbb{R}^{1\times T}$ denotes the charging profile of aggregator i, $\|\cdot\|_2$ denotes the Euclidean norm, $\mathbf{1}$ is the column vector of M_i ones, and $\mathbf{P}_{V_i} = \left[\mathbf{P}_{V_{i,1}}, \ldots, \mathbf{P}_{V_{i,M_i}}\right]^\intercal$ is the matrix of charging power of the PEVs in aggregator i, where M_i is the number of PEVs and $\mathbf{P}_{V_{i,n}} \in \mathbb{R}^{1\times T}, n = 1, \ldots, M_i$, is the charging profile of PEV n in aggregator i. The constraints of the network and the aggregated vehicles charging are represented by indicator functions $\mathbb{I}_N$ and $\mathbb{I}_{V_i}$:

$$\mathbb{I}_N = \begin{cases} 0, & \mathbf{P}_{\text{agg}_i} \in \mathcal{F}_N \\ \infty, & \text{otherwise} \end{cases} \tag{25}$$

$$\mathbb{I}_{V_i} = \begin{cases} 0, & \mathbf{P}_{V_{i,n}} \in \mathcal{F}_V \\ \infty, & \text{otherwise} \end{cases}. \tag{26}$$

This reformulated ADMM-based MOPF (called ADMM-BFM in the sequel) decomposes the original problem into two parts, *i.e.*, one for the network and another one for the PEVs, and solves them iteratively. The communication structure is shown in Fig. 2. In iteration k, the distribution system operator (DSO) performs the OPF calculation and transmits the charging signals, $\mathbf{P}_{\text{agg}_i}^{k+1}$, to the PEV aggregators. Then each aggregator dispatches the charging commands, $\mathbf{P}_{V_i}^{k+1}$, to every individual PEV that is managed by the aggregator. Finally, the DSO updates the dual variables u^{k+1}. As the iterates proceed, the power flow of the distribution network and the charging profile of the PEV fleet will reach optimality.

It is obvious that the solution to (22) only depends on the scale of a distribution network, but not relevant to the number of PEVs participating in charging control. On the other hand, the minimization problem (23) is a constrained quadratic

programming. In this iterative way, the memory use and the computational burden can be reduced to a large extent.

C. Aggregator Charging Power Minimization Step

Although (23) can be efficiently solved via quadratic programming solvers, e.g., Gurobi [40], the Hessian needs to be computed and stored when the number of variables and constraints explodes, which would cause prohibitively high time and storage consumption. Therefore we seek some way to address this issue.

It is pointed out in [39] that even when the x- and z-minimization steps in (20) are inexactly solved, ADMM will also converge as the iterations proceed. In this part, we exploit the special structure in the second step of ADMM-BFM and develop an approximate model that can be solved more efficiently than the original problem. First, we transform (23) into the following form:

$$\begin{aligned} \min_{\{\mathbf{x}_t\}} \quad & \sum_{t=1}^{T} f(\mathbf{x}_t; a_t) \\ \text{s.t.} \quad & 0 \le \mathbf{x}_t \le \mathbf{b}_t, \quad t = 1, \dots, T \\ & \sum_{t=1}^{T} \mathbf{x}_t = \mathbf{c} \end{aligned} \tag{27}$$

where $\mathbf{x}_t \in \mathbb{R}^M$, $\mathbf{b}_t \in \mathbb{R}^M$ and $\mathbf{c} \in \mathbb{R}^M$ are vectors, $a_t \ge 0$ is a scalar, and $f(\mathbf{x}_t; a_t) = (\mathbf{1}^\intercal \mathbf{x}_t - a_t)^2$ denotes the cost function at time t.

We construct a function as follows

$$g(\mathbf{x}_t; a_t) = M \sum_{i=1}^{M} \left(x_{i,t} - \frac{a_t}{M} \right)^2, \tag{28}$$

and substitute it into (27) as the surrogate objective function, then the minimization problem is cast as the Euclidean projection onto a simplex with box constraints, *i.e.,*

$$\begin{aligned} \min_{\{\mathbf{x}_t\}} \quad & \sum_{t=1}^{T} M \left\| \mathbf{x}_t - \mathbf{v}_t \right\|_2^2 \\ \text{s.t.} \quad & 0 \le \mathbf{x}_t \le \mathbf{b}_t, \quad t = 1, \dots, T \\ & \sum_{t=1}^{T} \mathbf{x}_t = \mathbf{c} \\ & \mathbf{v}_{i,t} = \frac{a_t}{M}, \quad \begin{matrix} i = 1, \dots, M \\ t = 1, \dots, T \end{matrix} . \end{aligned} \tag{29}$$

In the following, we will illustrate that the solution of formulation (29) is nearly optimal to that of problem (27).

Theorem 1 [41]: (*Objective Function Approximation*) Consider the two constrained optimization problems as follows:

$$\min f(x), \quad \text{s.t.} \quad x \in \mathcal{X} \tag{P}$$

$$\min \tilde{f}(x), \quad \text{s.t.} \quad x \in \mathcal{X} \tag{$\tilde{\text{P}}$}$$

where $\mathcal{X}$ is a non-empty set and f and $\tilde{f}$ are real-valued functions bounded below on $\mathcal{X}$. (P) is represented as the true problem and ($\tilde{\text{P}}$) as the approximate problem. If there exist scalars $\underline{\epsilon}$ and $\overline{\epsilon}$ satisfying

$$-\underline{\epsilon} \le \tilde{f}(x) - f(x) \le \overline{\epsilon} \quad \text{for all } x \in \mathcal{X}. \tag{30}$$

Then

$$-\underline{\epsilon} \le \inf_{x \in \mathcal{X}} \tilde{f}(x) - \inf_{x \in \mathcal{X}} f(x) \le \overline{\epsilon} \tag{31}$$

and for any $\epsilon \ge 0$, any ϵ-optimal solution $\tilde{x}$ to $\tilde{\text{P}}$ will necessarily be $(\epsilon + \underline{\epsilon} + \overline{\epsilon})$-optimal in (P).

Proof: See Appendix A. ■

Theorem 2: If the parameters in (27) satisfy

$$\epsilon = -\frac{1}{T} \Big(\sum_{i=1}^{M} c_i \Big)^2 + M \sum_{t=1}^{T} \sum_{i=1}^{M} b_{t,i}^2 \ge 0, \tag{32}$$

then the optimal solution to (29) is ϵ-optimal in (27).

Proof: See Appendix B. ■

Theorem 2 indicates that the projection problem (29) provides an near-optimal solution of (27) with an optimality gap ϵ that is relevant to the model parameters.

As is obviously observed from (29), the objective function and constraints are separable across rows with respect to $\mathbf{x}$, therefore the problem can be easily decomposed into M subproblems for $i = 1, \dots, M$:

$$\begin{aligned} \{x_{i,1}, \dots, x_{i,T}\} = \operatorname{argmin} \Bigg\{ & \sum_{i=1}^{T} M \big(x_{i,t} - \frac{a_t}{M} \big)^2 \\ & \text{subject to } \; 0 \le x_{i,t} \le b_{i,t}, \; t = 1, \dots, T \\ & x_{i,1} + x_{i,2} \cdots x_{i,T} = c_i \Bigg\} \end{aligned} \tag{33}$$

and be solved by Algorithm 1 [42] in a parallel manner, which would achieve dramatically more speed-up. See Appendix C for the procedures of the projection algorithm.

IV. Case Studies

In this section, we conduct some case studies in the IEEE 34-bus test feeder shown in Fig. 3, and the network parameters can be found in [43]. Since the IEEE network is a unbalanced three-phase radial network with regulators, transformers and distributed loads that are not modelled in this work, we make the same modifications as in [8]: 1) assume that each bus has three phases and split its spot load evenly in each phase; 2) model the distributed load on a line as two identical spot loads located at two ends of the line.

The maximum charging power is set to 10 kW and the battery capacity is 20 kWh. The initial and expected SOCs of all PEVs are uniformly sampled from the range $[20\%, 40\%]$ and $[80\%, 90\%]$, respectively. The charging efficiency of the PEV charging equipment is set to be 90% [44], [45]. In practice, the modelling of PEV users' behavior requires field data, whereas these data are difficult to fetch at present. To resolve this issue, the probability distribution functions are often used to sample the data. In this paper, the uniform distributions $U[16, 18]$ and $U[6, 9]$, as mentioned in [28], are adopted to randomly generate the arrival times and departure times. The daily load power profile is extracted from the UK national grid in 2016 [46]. To reflect the characteristics of the routine of residential power consumption, we respectively select one daily load profile in different time of the year, and scale down the maximum power to 1, as shown in Fig. 4.

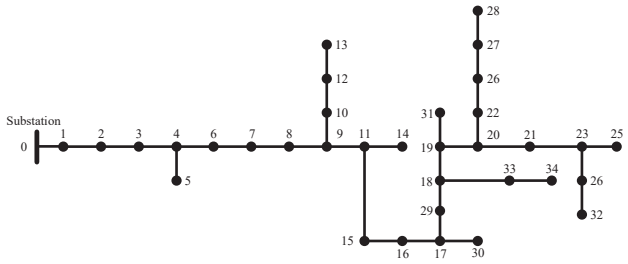

Fig. 3. Modified IEEE 34 bus test feeder.

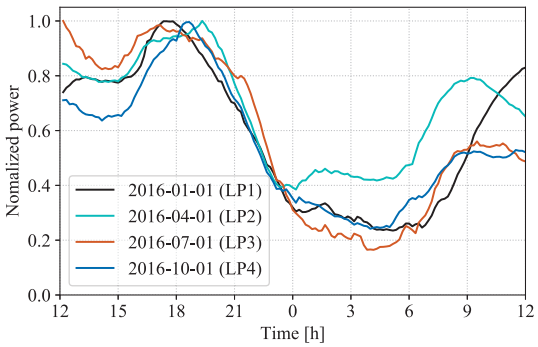

Fig. 4. Normalized daily load power profile.

TABLE I
COMPARISON RESULTS FOR DIFFERENT SIZES OF PROBLEM

M	Time [s]			Objective Value		
	Proj(1)[a]	Proj(4)[b]	Gurobi	Projection	Gurobi	Error [%]
100	0.035	0.091	0.566	223.035	221.773	0.568
500	0.167	0.127	2.812	1126.153	1104.965	1.917
1000	0.334	0.174	5.540	2234.345	2209.923	1.105
2000	0.656	0.264	17.304	4466.079	4419.846	1.046
5000	1.636	0.554	32.679	11159.534	11048.676	1.003
10000	3.260	1.043	66.273	28471.532	28072.124	1.422

[a] Serial implementation of projection algorithm.
[b] Parallel implementation with 4 threads.

The time interval Δt is set to 10 minutes and the scheduling horizon is sliced into $T = 144$ time slots.

The model formulations are implemented using the open-source package JuMP [47] and solved on Windows 10 64-bit system with an Intel Core i5-4590 processor with 8GB RAM using Ipopt [48] version 3.12.2 to solve MOPF problem (22).

A. Verification of the Projection Algorithm

Some experiments are conducted with various sizes of the the variables so as to compare the accuracy of the reformulated problem (29) solved by the proposed projection algorithm to the original problem (27) solved by the interior point method in Gurobi [40] with the default solver parameters. In all cases, the parameter setup is as follows: time slots $T = 144$, the entries of $\mathbf{c}$ are all 20, $\mathbf{b}$ is constructed from (14) with maximum value 10, and $\mathbf{a}$ is set as $M/2$ times as the normalized load power shown in Fig. 4.

Table I displays the solution time and objective values of (27) for different values of M. Note that in the table are provided the results of projection algorithm for serial and parallel implementations, respectively. As can be observed in all cases, the projection algorithm can reach an approximate solution close to the optimum with a small relative error of the objective value, while the solution time spent is only 1/20 of that of Gurobi. It reveals that the proposed projection algorithm can provide a solution to sufficient precision.

The reason why the parallel version of projection algorithm is slower than the serial version when M is small lies in that the communication time among CPU cores predominates in the total runtime, whereas it takes up smaller proportion when M gets larger, thus making the parallel version over two times as fast as the serial version.

Note that in our work, 4 cores at the most can be used due to the limitation of computing resource. Thus the solution time can be further reduced if more CPU cores are available.

TABLE II
TYPE OF LOAD PROFILE FOR DIFFERENT BUSES

Bus number	Type of load profile
3,4,5,6,10,11	LP1
12,13,14,15,16,17	LP2
18,19,20,21,22,25	LP3
27,29,31,32,35	LP4

B. Optimality of ADMM-BFM

In this part, we investigate the optimality performance of the proposed solution method (ADMM-BFM) compared to the original method (BFM). The load profiles at different buses are categorized into four types that are shown in Fig. 4 and the bus indices for each type are listed in Table II. Besides, the line current limit is set as 80 A. The charging profiles of PEV aggregator for different algorithms, *i.e.*, BFM, ADMM-BFM and dumb control, are compared. The term *dumb control* is referred to as the circumstance that a PEV starts to charge upon its arrival until fully charged and no active control is imposed in the duration. The profile given by BFM is regarded as the baseline to assess the accuracy of solution by ADMM-BFM.

Up to the present time, there is few literature discussing the parameter selection of the ADMM. In [49], a specific parameter selection method is proposed for the ADMM-like problems that are of quadratic form, and it's proved to lead to optimal solution. However, in the general case, there are no general rules of how to select the optimal penalty parameter ρ. Therefore in the present work we choose ρ by trial and errors. We find that when ρ falls in the inverval $[0.5, 3]$, the iterates can guarantee the convergence and yield the same optimal objective value.

(a) Single aggregator

In this scenario, a PEV aggregator that comprises of 300 PEVs is located at bus 11. Fig. 5 shows the curves of substation power and aggregator charging power in 24 hours. From the figure, one can observe that ADMM-BFM obtains a charging profile close to BFM with a relative error of 0.012%, and the objective values are 27.570899 MWh and 27.570899 MWh, respectively. It indicates that the proposed ADMM-BFM is capable of providing a considerably approximate solution. The runtime of BFM is 4.59 seconds while it takes 27.46 seconds within 5 iterations for ADMM-BFM. In

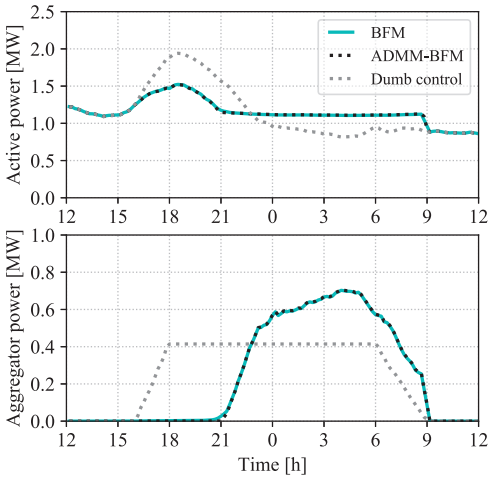

Fig. 5. Daily profile of substation power and aggregator charging power by different control algorithms.

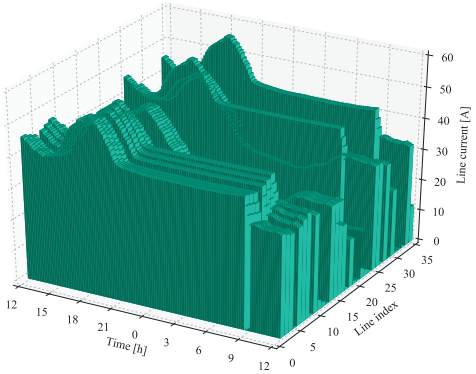

Fig. 6. Current flows in each line across the 24 hours.

this case the performance of BFM is superior to ADMM-BFM due to the small number of PEVs, however the solution time of BFM will increase dramatically with the number of PEVs, while that of ADMM-BFM can keep slower increase. In the next subsection, it will be demonstrated in details.

Fig. 6 shows the current in each transmission line across the scheduling time. We can see that the line current is below the limit (60 A) at any time. The maximum line current is 56.54 A that occurs at time t=18:30 in the line 1-2.

In comparison to dumb control, the generation cost minimization control strategy considers the requirements of the distribution network on a higher level, which results in the PEVs charging during the off-peak hours and therefore reducing the peak power. Moreover, the variation of the power at the substation is suppressed, and accordingly the network energy loss is reduced by 4% from 0.2125 MWh to 0.2038 MWh.

(b) Multiple aggregators

In this case, three aggregators with each containing 100 PEVs are located at buses 11, 17 and 21, being denoted as Agg1, Agg2 and Agg3, respectively. The other settings are the same as the single-aggregator case.

The optimization process converges after 3 iterations and takes 16.43 seconds. The optimal objective value is 27.5804

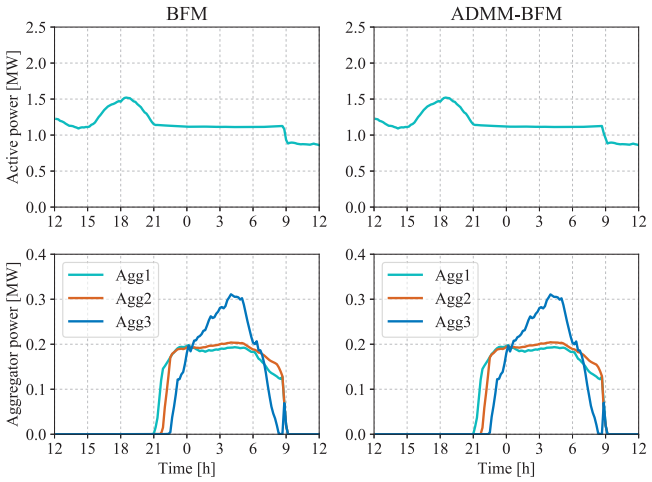

Fig. 7. Daily profile of substation power and aggregator charging power by BFM (*left*) and ADMM-BFM (*right*) in multiple-aggregator case.

TABLE III
COMPUTATIONAL PERFORMANCE OF THE BI-LEVEL DECOMPOSITION METHOD IN [32].

Penalty Coefficient	Iterations	Objective Value [MWh]	Runtime [s]
1	10	27.58063	160.89
2	25	27.58056	225.03
3	37	27.58050	596.03
4	53	27.58045	1052.66

MWh. Fig. 7 shows the charging profile of each aggregator by BFM and ADMM-BFM. The relative errors are 0.0946%, 0.156% and 0.0873%, respectively. The network energy loss is 0.2133 MWh, a bit larger than the single-aggregator case. The reason appears to be that Agg2 and Agg3 are located at the buses that are further from the substation, thus leading to more energy losses on the transmission lines.

(c) Comparison with the method in [32]

The bi-level decomposition method in [32] is similar to ours, but the solution performance is sensitive to the value of penalty coefficient. As show in Table III, the larger the penalty coefficient, the closer the obtained optimal objective value to that of the ADMM-BFM, but more number of iterations and computation time is needed to converge. Compared with the bi-level programming method in [32], the ADMM-BFM in our work shows better convergence performance.

C. Runtime Performance

With the increase in the population of PEVs, the variables and constraints of the optimization problem will become prohibitively large, which could degrade the solution efficiency. Therefore in this part, the scheduling problem of different numbers of PEVs M, ranging from 100 to 50k, is solved by BFM and ADMM-BFM for ten times, and the average runtime versus the values of M is depicted in Fig. 8. Both of BFM and ADMM-BFM display linear performance in time as expected, nevertheless ADMM-BFM has a relatively flatter slope that is about the third of BFM. When M is small (<5k

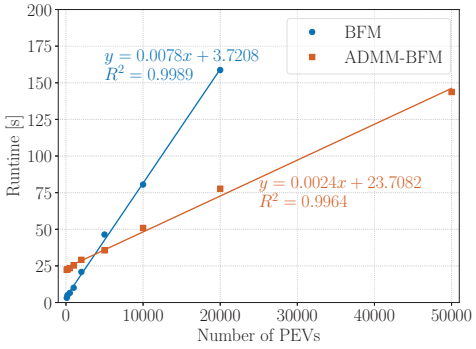

Fig. 8. Runtime performances for different numbers of PEVs by BFM and ADMM-BFM.

herein), BFM shows superior performance, whereas ADMM-BFM outperforms BFM when M becomes considerably large. Specifically, when $M = 50$k BFM fails to solve due to memory overflow, but ADMM-BFM still maintains good performance. This implies that ADMM-BFM is well suited for a large-scale scenario where tens of thousands of PEVs are integrated into a network.

It is noteworthy that in real practice the projection algorithm can be carried out locally by each PEV itself and then sends the optimal charging profile back to the aggregator. Thus the time consumption of each iteration of ADMM-BFM is a total of the time to solve MOPF, the time to solve only one subproblem (33) and signal transmission time, which would result in more reduction in runtime and memory footprint.

D. 119-Bus Case

A larger distribution network with 119 buses [50] is utilized to test the scalability of the proposed ADMM-BFM. The system operates at 11 kV with 22.809 MW and 17.041 Mvar loads. The structure of the 119-bus test feeder system is illustrated in Fig. 9, and the parameters of line impedance and load power are given in reference [50]. Some modifications are made: (i) four PEV aggregators are installed on buses 21, 51, 75, 112, and the number of PEVs in each aggregator is 4000, 5000, 3000 and 6000; (ii) the load power on all buses except the root bus changes according to the load profile in Fig. 4.

In this case, the parameters are set as follows: $\rho = 1.5$ and $\epsilon^{\text{prim}} = \epsilon^{\text{dual}} = 0.01$. Shown in Fig. 10(a) is the charging power of four aggregators after 100 iterations. The relative errors between the required power and practical power for each aggregator, $\|P_{\text{agg}} - \hat{P}_{\text{agg}}\|/\|P_{\text{agg}}\|$, are shown in Fig. 10(b). The maximum relative error, about 1%, occurs in Agg21, and the errors of the other aggregators are less than 0.1%. In real practice, these errors are acceptable. It can be observed from Fig. 10(c) that the norms of primal residual and dual residual converge to stationary values as iteration counts increase. Fig. 10(d) shows the objective value reach suboptimality within 30 iterations that take about 630 seconds to carry out.

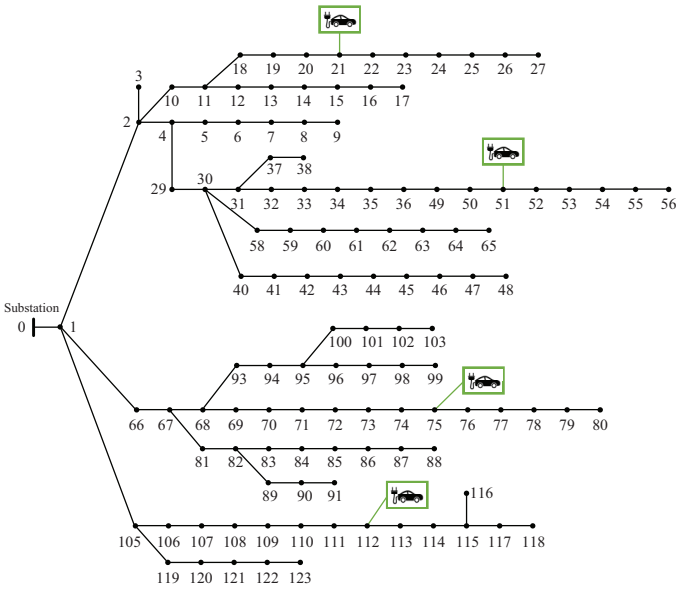

Fig. 9. Modified 119 bus test feeder [50].

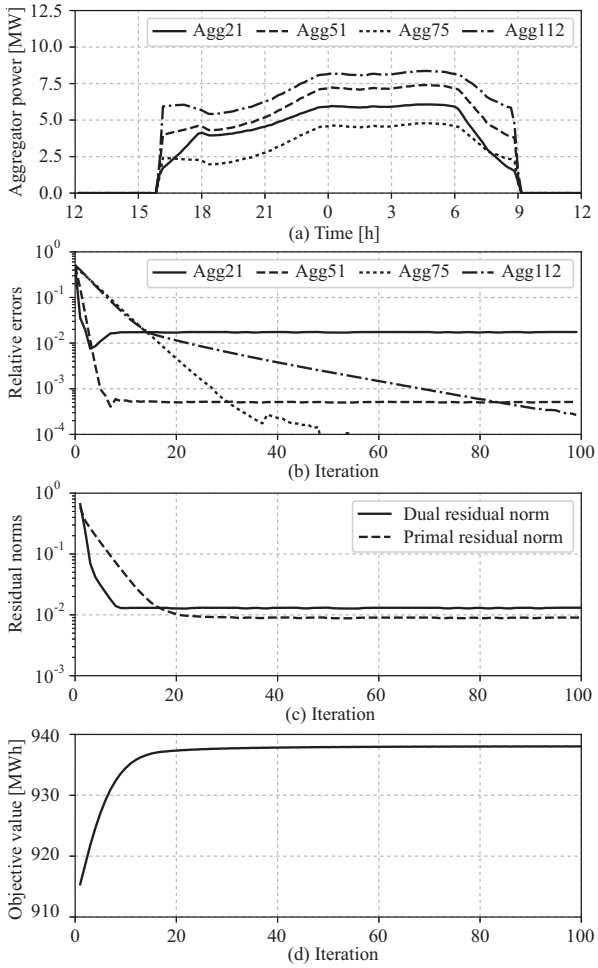

Fig. 10. Charging profile of aggregators and iteration process in the 119-bus case. (a) The charging power of the four aggregators during the scheduling period; (b) Relative errors between required power and practical power for each aggregator; (c) Norms of primal residual and dual residual per iteration; (d) Objective value per iteration.

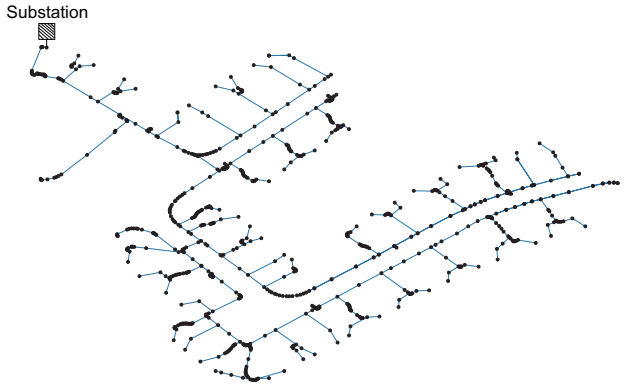

Fig. 11. The geographical structure of the European low voltage network with 906 buses. Each black dot indicates a bus.

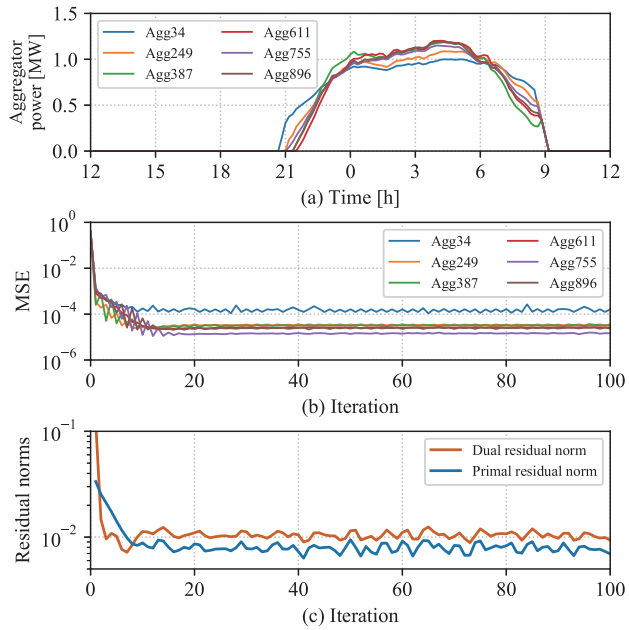

Fig. 12. Charging profile of aggregators and iteration process in the European case. (a) The charging power of the six aggregators during the scheduling period; (b) Mean squared error of the charging power of each aggregator; (c) Norms of primal residual and dual residual per iteration.

E. 906-Bus Case

To further validate the applicability of the proposed approach in practical distribution network, the IEEE European low-voltage test feeder [43] is modified for use in the simulations. This network comprises of 906 buses and 55 loads and operates at 240 V. In the modified network, we assume that 6 PEV aggregators are located at buses 34, 249, 387, 611, 755 and 896, and 500 PEVs are managed in each aggregator, respectively. At every iteration of the ADMM-BFM, the mean squared error (MSE) of each aggregator power compared with the aggregator power obtained by the BFM is depicted in Fig. 12 (b), which validates again that the ADMM-BFM can achieve the optimum. The optimal objective value is 321.020592 MWh and 321.018286 MWh respectively for the BFM and the ADMM-BFM. As can be seen from Fig. 12 (b) and (c), the iterates converge after tens of times.

V. Discussion

All of the three simulations cases demonstrate the ADMM-BFM outperforms the original BFM in computational cost and can reach the optimal solution with high precision. Moreover, this proposed method works well in the radial distribution network, either MV network or LV network.

However, there are still some problems to settle. First, the proposed MOPF model does not consider the control of transformer. Due to the discrete property of tap-changer, the MOPF problem would be cast into a discrete optimization problem. The present algorithm is not able to solve such a mixed integer programming problem. Second, because of the nonconvexity of the MOPF model, only near-optimal solution can be guaranteed. Nonetheless, the simulation results have shown decent property of convergence and the optimal solution obtained with the BFM and the ADMM-BFM coincides. Third, under the objective of minimizing the overall energy consumption, it is likely to lead to frequent connections/disconnections of PEVs when the load profile is changing rapidly, thus inflicting significant damage on the batteries.

To resolve the above three issues in the future work, we will take into account regulators and transformers to improve the algorithm, and conduct further study on what constraints need to be imposed on the charging process of PEVs and on the theoretical conditions of the global optimum of the ADMM-BFM.

VI. Conclusion

In this paper, we propose a distributed algorithm based on the ADMM framework to solve the multiperiod optimal power flow problem that takes into account the charging of large-scale population of PEVs. Under the circumstances that tens of thousands of PEVs participates in the charging control, the original problem would be difficult to solve via interior point method in a centralized way. Therefore we take advantage of the decomposability of ADMM and resolve the original problem into two subproblems that can be solved in an iterative manner. In the first subproblem, the PEVs located on one bus are viewed as a whole and an aggregator is established to manage them. Then the MOPF problem is solved to allocate charging power to each PEV aggregator. The second subproblem is a constrained quadratic program and is aimed at dispatching the total power of aggregator obtained in the previous step to each PEV. As the iterates progress, the problem converges to optimality.

To accelerate solution of the second subproblem, we use a function to approximate its objective function and the surrogate subproblem turns out to be a problem of Euclidean projection onto a simplex with box constraints. The proof is given that the surrogate subproblem provides an ϵ-optimal solution to the original one as long as certain conditions hold. The surrogate problem is solved efficiently by a projection algorithm that can be implemented in parallel. The numerical studies demonstrate a negligible relative error and high solution efficiency as compared to the original subproblem.

In comparison to BFM, the proposed ADMM-BFM can reach optimality in considerably less time and with memory

use. Besides, ADMM-BFM is easily scalable in larger networks, whereas BFM may fail due to memory limitation. In the next research work, we will devote to relaxing the nonconvex BFM to second-order cone program that is convex and easy to solve by state-of-the-art SOC solver, and to exploring the recovery conditions under which the relaxation has zero-gap optimality. It is promising for the relaxed version of ADMM-BFM to achieve further speed-up while assuring high accuracy.

APPENDIX A
PROOF OF THEOREM 1

Proof: The inequalities (31) can be easily obtained by rewriting (30) as

$$f(x) \le \tilde{f}(x) + \underline{\epsilon}$$
$$\tilde{f}(x) \le f(x) + \overline{\epsilon}.$$

Then we can obtain the two inequalities below, and combining them yields (31).

$$\inf_{x\in\mathcal{X}} f(x) \le \inf_{x\in\mathcal{X}} \tilde{f}(x) + \underline{\epsilon}$$
$$\inf_{x\in\mathcal{X}} \tilde{f}(x) \le \inf_{x\in\mathcal{X}} f(x) + \overline{\epsilon}.$$

Now let $\tilde{x}$ be an ϵ-optimal solution to $\tilde{\mathrm{P}}$ for some $\epsilon \ge 0$. Then we have

$$\begin{aligned} f(\tilde{x}) &\le \tilde{f}(\tilde{x}) + \underline{\epsilon} \\ &\le \inf_{x\in\mathcal{X}} \tilde{f}(x) + \epsilon + \underline{\epsilon} \\ &\le \inf_{x\in\mathcal{X}} f(x) + \epsilon + \underline{\epsilon} + \overline{\epsilon}, \end{aligned}$$

therefore $\tilde{x}$ is $(\epsilon + \underline{\epsilon} + \overline{\epsilon})$-optimal in (P). ■

APPENDIX B
PROOF OF THEOREM 2

Proof: Let $\mathbf{x}^\star$ be the optimal solution of (29). By subtracting g from f and summing over t, we have

$$\begin{aligned} \Delta &= \sum_{t=1}^{T} \big(f(x_t^\star) - g(x_t^\star)\big) \\ &= \sum_{t=1}^{T} \big(\sum_{i=1}^{M} x_{i,t}^\star\big)^2 - M \sum_{t=1}^{T}\sum_{i=1}^{M} x_{i,t}^{\star 2}. \end{aligned} \tag{34}$$

According to Cauchy-Schwarz inequality and the constraints on $\mathbf{x}$, the following inequalities hold.

$$\big(\sum_{i=1}^{M} x_{i,t}^\star\big)^2 \le M \sum_{i=1}^{M} x_{i,t}^{\star 2}$$
$$\frac{1}{T}\big(\sum_{i=1}^{M} c_i\big)^2 \le \sum_{t=1}^{T} \big(\sum_{i=1}^{M} x_{i,t}^\star\big)^2 \le \sum_{t=1}^{T} \big(\sum_{i=1}^{M} b_{i,t}\big)^2$$
$$\frac{M}{T}\big(\sum_{i=1}^{M} c_i\big)^2 \le M \sum_{t=1}^{T}\sum_{i=1}^{M} x_{i,t}^{\star 2} \le M \sum_{t=1}^{T}\sum_{i=1}^{M} b_{i,t}^2$$

Hence, we can get

$$-\epsilon \le \Delta \le 0, \tag{35}$$

if $\epsilon \ge 0$. Applying Theorem 1 yields that $\mathbf{x}^\star$ is an ϵ-optimal solution to (27). This completes the proof. ■

Algorithm 1 Algorithm for Euclidean projection onto a simplex with box constraints.

Input: $\mathbf{v}$, upper bounds $\mathbf{b}$ and simplex constraint c.

Construct the set $\mathcal{W} = \{v_1, \dots, v_n, v_1 - b_1, \dots, v_n - b_n\}$.
Construct the set $\mathcal{V} = \{v_1, \dots, v_n\}$.
$s_{\text{all}} \leftarrow \text{sum}(\mathbf{v})$, $s_l \leftarrow 0$, $s_c \leftarrow 0$, $n_l \leftarrow 0$, $n_c \leftarrow 0$.
while $|\mathcal{W}| > 2$ **do**
  $\theta_p \leftarrow \text{median}(\mathcal{W})$.
  Use θ_p to partition $\mathcal{W}$ into three index sets $\mathcal{S}_l$, $\mathcal{S}_u$ and $\mathcal{S}_c$ by equation (36).
  $\bar{n}_l \leftarrow |\mathcal{V}_{\mathcal{S}_l}|$, $\bar{s}_l \leftarrow \text{sum}(\mathcal{V}_{\mathcal{S}_l})$, $\bar{n}_c \leftarrow |\mathcal{V}_{\mathcal{S}_c}|$, $\bar{s}_c \leftarrow \text{sum}(\mathcal{V}_{\mathcal{S}_c})$.
  $c_p \leftarrow s_{all} - s_l - s_c - \theta_p(n - n_l - n_c)$
    $-\bar{s}_l - \bar{s}_c + \theta_p(\bar{n}_l + \bar{n}_c)$
  if $c_p > c$ **then**
    $n_l \leftarrow n_l + \bar{n}_l$, $s_l \leftarrow s_l + \bar{s}_l$.
    Delete the entries greater than θ_p in $\mathcal{W}$.
    $\mathcal{V} \leftarrow \mathcal{V} \setminus \mathcal{V}_{\mathcal{S}_l}$.
  else if $c_p < c$ **then**
    $n_c \leftarrow n_c + \bar{n}_c$, $s_c \leftarrow s_c + \bar{s}_c$.
    Delete the entries smaller than θ_p in $\mathcal{W}$.
    $\mathcal{V} \leftarrow \mathcal{V} \setminus \mathcal{V}_{\mathcal{S}_c}$.
  else
    $\theta^* \leftarrow \theta_p$.
    return $\mathbf{x}$ using (36).
  end if
end while
$\theta_p \leftarrow \max(\mathcal{W})$ and obtain $\mathcal{S}_l$, $\mathcal{S}_u$ and $\mathcal{S}_c$.
$\theta^* \leftarrow \dfrac{|\mathcal{S}_c| + \text{sum}(\mathcal{V}_{\mathcal{S}_u}) - c}{|\mathcal{S}_u|}$.
return $\mathbf{x}$ using (36).

APPENDIX C

Given the following Euclidean projection problem

$$\begin{aligned} \min_{\mathbf{x}} \quad & \|\mathbf{x} - \mathbf{v}\|_2^2 \\ \text{s.t.} \quad & 0 \le \mathbf{x} \le \mathbf{b} \\ & \sum_{i=1}^{n} x_i = c \end{aligned}$$

where $\mathbf{v}, \mathbf{b} \in \mathbb{R}^n$ are parameter vectors.

We first obtain the pivot value θ from the merged array $[\mathbf{v}, \mathbf{v} - \mathbf{b}]$ via bisection search method, then use θ to partition the indices of $[\mathbf{v}, \mathbf{v} - \mathbf{b}]$ into three sets $(\mathcal{S}_l, \mathcal{S}_u, \mathcal{S}_c)$, and evaluate the corresponding values of x_i for $i = 1, \dots, n$ as follows

$$x_i = \begin{cases} 0, & \text{if } v_i \le \theta \quad (\mathcal{S}_l) \\ b_i, & \text{if } v_i \ge b_i + \theta \quad (\mathcal{S}_u) \\ v_i - \theta, & \text{otherwise} \quad (\mathcal{S}_c). \end{cases} \tag{36}$$

REFERENCES

[1] B. Stott and O. Alsac, "Fast decoupled load flow," *IEEE Trans. Power App. Syst.*, vol. PAS-93, no. 3, pp. 859–869, May 1974.

[2] O. Alsaç, J. Bright, M. Prais, and B. Stott, "Further developments in LP-based optimal power flow," *IEEE Trans. Power Syst.*, vol. 5, no. 3, pp. 697–711, Aug. 1990.

[3] J. Lavaei, S. Member, and S. H. Low, "Zero duality gap in optimal power flow problem," *IEEE Trans. Power Syst.*, vol. 27, no. 1, pp. 92–107, Jan. 2012.

[4] D. K. Molzahn, S. Member, J. T. Holzer, B. C. Lesieutre, S. Member, and C. L. Demarco, "Implementation of a large-scale optimal power flow solver based on semidefinite programming," *IEEE Trans. Power Syst.*, vol. 28, no. 4, pp. 3987–3998, Nov. 2013.

[5] M. S. Andersen, A. Hansson, and L. Vandenberghe, "Reduced-complexity semidefinite relaxations of optimal power flow problems," *IEEE Trans. Power Syst.*, vol. 29, no. 4, pp. 1855–1863, Jul. 2014.

[6] M. Farivar and S. Low, "Branch flow model: Relaxations and convexification–part I," *IEEE Trans. Power Syst.*, vol. 28, no. 3, pp. 2554–2564, Aug. 2013.

[7] M. Farivar and S. Low, "Branch flow model: Relaxations and convexification–part II," *IEEE Trans. Power Syst.*, vol. 28, no. 3, pp. 2565–2572, Aug. 2013.

[8] L. Gan, N. Li, U. Topcu, and S. H. Low, "Exact convex relaxation of optimal power flow in radial networks," *IEEE Trans. Autom. Control*, vol. 60, no. 1, pp. 72–87, Jan. 2015.

[9] D. K. Molzahn and I. A. Hiskens, "Moment-based relaxations of the optimal power flow problem," in *SIAM Conf. Comput. Sci. Eng.*, Salt Lake City, UT, Mar. 2014.

[10] D. K. Molzahn and I. A. Hiskens, "Sparsity-exploting moment-based relaxations of the optimal power flow problem," *IEEE Trans. Power Syst.*, vol. 30, no. 6, pp. 3168–3180, Nov. 2015.

[11] C. Josz, J. Maeght, P. Panciatici, and J. C. Gilbert, "Application of the moment-SOS approach to global optimization of the OPF problem," *IEEE Trans. Power Syst.*, vol. 30, no. 1, pp. 463–470, Jan. 2015.

[12] C. Duan, L. Jiang, W. Fang, and J. Liu, "Moment-SOS approach to interval power flow," *IEEE Trans. Power Syst.*, vol. 32, no. 1, pp. 522–530, Jan. 2017.

[13] C. Coffrin, H. L. Hijazi, P. V. Hentenryck, and C. E. Feb, "The QC relaxation: Theoretical and computational results on optimal power flow," *IEEE Trans. Power Syst.*, vol. 31, no. 4, pp. 3008–3018, Jul. 2016.

[14] D. K. Molzahn and I. A. Hiskens, "Mixed SDP/SOCP moment relaxations of the optimal power flow problem," in *IEEE PowerTech*, Eindhoven, Netherlands, 2015, pp. 1–6.

[15] S. Bose, S. H. Low, T. Teeraratkul, and B. Hassibi, "Equivalent relaxations of optimal power flow," *IEEE Trans. Autom. Control*, vol. 60, no. 3, pp. 729–742, Mar. 2015.

[16] S. H. Low, "Convex relaxation of optimal power flow part I: Formulations and equivalence," *EEE Trans. Control Network Syst.*, vol. 1, no. 1, pp. 15–27, Mar. 2014.

[17] B. Kocuk, S. S. Dey, and X. A. Sun, "Inexactness of SDP relaxation and valid inequalities for optimal power flow," *IEEE Trans. Power Syst.*, vol. 31, no. 1, pp. 642–651, Jan. 2016.

[18] D. K. Molzahn, I. A. Hiskens, and P. P. Member, "A Laplacian-based approach for finding near globally optimal solutions to OPF problems," *IEEE Trans. Power Syst.*, vol. 32, no. 1, pp. 305–315, Jan. 2016.

[19] Y. C. Wu, A. S. Debs, and R. E. Marsten, "A direct nonlinear predictor-corrector primal-dual interior point algorithm for optimal power flows," *IEEE Trans. on Power Syst.*, vol. 9, no. 2, pp. 876–883, 1994.

[20] F. Capitanescu and L. Wehenkel, "Experiments with the interior-point method for solving large scale optimal power flow problems," *Electr. Power Syst. Res.*, vol. 95, no. 2, pp. 276–283, 2013.

[21] C. Duan, W. Fang, L. Jiang, and J. Liu, "Adaptive barrier filter-line-search interior point method for optimal power flow with FACTS devices," *IET Gener. Transm. Distrib.*, vol. 9, no. 16, pp. 2792–2798, 2015.

[22] W. A. Bukhsh, A. Grothey, K. I. M. Mckinnon, and P. A. Trodden, "Local solutions of the optimal power flow problem," *IEEE Trans. Power Syst.*, vol. 28, no. 4, pp. 4780–4788, 2013.

[23] N. Alguacil and A. J. Conejo, "Multiperiod optimal power flow using benders decomposition," *IEEE Trans. Power Syst.*, vol. 15, no. 1, pp. 196–201, Feb. 2000.

[24] R. A. Jabr, S. Karaki, and J. A. Korbane, "Robust multi-period OPF with storage and renewables," *IEEE Trans. Power Syst.*, vol. 30, no. 5, pp. 2790–2799, Sep. 2014.

[25] A. O'Connell, D. Flynn, and A. Keane, "Rolling multi-period optimization to control electric vehicle charging in distribution networks," *IEEE Trans. Power Syst.*, vol. 29, no. 1, pp. 340–348, Jan. 2014.

[26] R. A. Jabr, "Minimum loss operation of distribution networks with photovoltaic generation," *IET Renewable Power Gener.*, vol. 8, no. 1, pp. 33–44, May 2014.

[27] C. Duan, L. Jiang, W. Fang, and J. Liu, "Multi-period OPF with energy storages and renewable sources: A parallel moment approach," in *IEEE Power Energy Society General Meeting*. IEEE, 2016, pp. 1–5.

[28] A. Santos, N. McGuckin, H. Y. Nakamoto, D. Gray, and S. Liss, "Summary of travel trends: 2009 national household travel survey," Tech. Rep., 2011.

[29] E. Veldman and R. A. Verzijlbergh, "Distribution grid impacts of smart electric vehicle charging from different perspectives," *IEEE Trans. Smart Grid*, vol. 6, no. 1, pp. 333–342, Jan. 2015.

[30] L. Gan and S. Low, "Optimal decentralized protocols for electric vehicle charging," *IEEE Trans. Power Syst.*, vol. 28, no. 2, pp. 940–951, May 2013.

[31] I. Sharma, K. Bhattacharya, C. Canizares, and K. Bhattacharya, "Smart charging of PEVs penetrating into residential distribution systems," *IEEE Trans. Smart Grid*, vol. 5, no. 3, pp. 1196–1209, May 2014.

[32] W. Yao, J. Zhao, F. Wen, Y. Xue, and G. Ledwich, "A hierarchical decomposition approach for coordinated dispatch of plug-in electric vehicles," *IEEE Trans. Power Syst.*, vol. 28, no. 3, pp. 2768–2778, Aug. 2013.

[33] M. E. Baran and F. F. Wu, "Optimal capacitor placement on radial distribution systems," *IEEE Trans. Power Delivery*, vol. 4, no. 1, pp. 725–734, Jan. 1989.

[34] M. E. Baran and F. F. Wu, "Optimal sizing of capacitors placed on a radial distribution system," *IEEE Trans. Power Delivery*, vol. 4, no. 1, pp. 735–743, Jan. 1989.

[35] K. Christakou, D. C. Tomozei, J. Y. L. Boudec, and M. Paolone, "AC OPF in radial distribution networks - Part I: On the limits of the branch flow convexification and the alternating direction method of multipliers," *Electr. Power Syst. Res.*, vol. 143, pp. 438–450, 2017.

[36] Y. Cao, R. C. Kroeze, and P. T. Krein, "Multi-timescale parametric electrical battery model for use in dynamic electric vehicle simulations," *IEEE Trans. Transp. Electrif.*, vol. 2, no. 4, pp. 432–442, Dec. 2016.

[37] H. Chaoui, "State of charge and state of health estimation for lithium batteries using recurrent neural networks," *IEEE Trans. Veh. Technol.*, vol. PP, no. 99, pp. 1–1, Oct. 2017.

[38] L. F. Ochoa and G. P. Harrison, "Minimizing energy losses: Optimal accommodation and smart operation of renewable distributed generation," *IEEE Trans. Power Syst.*, vol. 26, no. 1, pp. 198–205, Feb. 2011.

[39] S. Boyd, N. Parikh, E. Chu, B. Peleato, and J. Eckstein, "Distributed optimization and statistical learning via the alternating direction method of multipliers," *Foundations Trends in Machine Learning*, vol. 3, no. 1, pp. 1–122, Jan. 2011.

[40] Gurobi Optimization, Inc., "Gurobi optimizer reference manual," 2015. [Online]. Available: http://www.gurobi.com

[41] A. M. Geoffrion, "Objective function approximations in mathematical programming," *Math. Program.*, vol. 13, no. 1, pp. 23–37, Dec. 1977.

[42] M. D. Gupta, S. Kumar, and J. Xiao, "L1 projections with box constraints," *arXiv: 1010.0141 [cs.DS]*, Sep. 2010.

[43] IEEE PES Distribution System Analysis Subcommittee's Distribution Test Feeder Working Group, "IEEE distribution test feeders." [Online]. Available: https://ewh.ieee.org/soc/pes/dsacom/testfeeders/

[44] P. Richardson, D. Flynn, and A. Keane, "Optimal charging of electric vehicles in low-voltage distribution systems," *IEEE Trans. Power Syst.*, vol. 27, no. 1, pp. 268–279, Feb. 2012.

[45] M. Zhang and J. Chen, "The energy management and optimized operation of electric vehicles based on microgrid," *IEEE Trans. Power Delivery*, vol. 29, no. 3, pp. 1427–1435, May 2014.

[46] UK National Grid, "G.B. National Grid Status," 2016. [Online]. Available: http://www.gridwatch.templar.co.uk

[47] M. Lubin and I. Dunning, "Computing in operations research using Julia," *INFORMS J. Comput.*, vol. 27, no. 2, pp. 238–248, Mar. 2015.

[48] A. Wächter and L. T. Biegler, "On the implementation of an interior-point filter line-search algorithm for large-scale nonlinear programming," *Math. Program.*, vol. 106, no. 1, pp. 25–57, Mar. 2006.

[49] E. Ghadimi, A. Teixeira, I. Shames, and M. Johansson, "Optimal parameter selection for the alternating direction method of multipliers (ADMM): Quadratic problems," *IEEE Trans. Autom. Control*, vol. 60, no. 3, pp. 644–658, Mar. 2013.

[50] D. Zhang, Z. Fu, and L. Zhang, "An improved TS algorithm for loss-minimum reconfiguration in large-scale distribution systems," *Electr. Power Syst. Res.*, vol. 77, no. 5, pp. 685–694, Apr. 2007.

Hua Fan received the B.S. and Ph.D. degrees from the School of Electrical and Electronic Engineering, Huazhong University of Science and Technology (HUST), Wuhan, China, in 2012 and 2017, respectively.

He was a Visiting Scholar at the University of Liverpool, UK, from May 2014 to May 2015. He joined the State Grid Zhejiang Information & Telecommunication Company, China in July 2017. His current research interests include electric spot market and optimization methods in power system.

Chao Duan (S'14) was born in Chongqing, China, in 1989. He received the B.S. degree in electrical engineering from Xi'an Jiaotong University, Xi'an, China, in 2012. He is currently pursuing the Ph.D. degree at Xi'an Jiaotong University, Xi'an, China, and the University of Liverpool, Liverpool, U.K.

His research interests are in stochastic optimization, stability analysis and robust control of power systems.

Chuan-Ke Zhang (S'12-M'14) received the B.S. degree in automation and the Ph.D. degree in control science and engineering from Central South University, Changsha, China, in 2007 and 2013, respectively.

He was a Research Assistant with the Department of Electrical Engineering and Electronics, University of Liverpool, Liverpool, U.K., from 2011 to 2013, where he was a Post-Doctoral Research Associate from 2014 to 2016. He joined the School of Automation, China University of Geosciences, Wuhan, China, in 2014, where he is currently an Associate Professor. His current research interests include time-delay systems, chaos synchronization, and power system stability and control.

Lin Jiang (M00) received the B.Sc. and M.Sc. degrees from Huazhong University of Science and Technology (HUST), China, in 1992 and 1996; and the Ph.D. degree from the University of Liverpool, UK, in 2001, all in Electrical Engineering.

Currently, he is a Reader in The University of Liverpool. His research interests include control and optimization of power system and smart grid with ICT, renewable energy generation and integration, and demand-side response. He is the associate editor of IET Renewable Power Generation, IET Smart Grid, and Protection and Control of Modern Power Systems.

Chengxiong Mao (M'93-SM'08) received the B.S., M.S., and Ph.D. degrees from the Department of Electrical Engineering, Huazhong University of Science and Technology (HUST), Wuhan, China, in 1984, 1987, and 1991, respectively.

He was a Visiting Scholar at the University of Calgary, Calgary, AB, Canada, from January 1989 to January 1990 and at Queen's University of Belfast, Belfast, U.K., from December 1994 to December 1995. He conducted research at the Technische Universitaet Berlin, Berlin, Germany, from April 1996 to April 1997 with the support of Humboldt Foundation. He is currently a Professor with HUST. His research interests include power system operation and control, excitation control of synchronous generators, and applications of high-power electronic technology to power systems.

Dan Wang (M'07-SM'17) received the B.S., M.S., and Ph. D. degrees from the Department of Electrical Engineering, Huazhong University of Science and Technology (HUST), Wuhan, China, in 1999, 2002, and 2006, respectively.

He was a Postdoctoral Researcher, from 2006 to 2008, sponsored by the China Postdoctoral Science Foundation in the Department of Control Science and Engineering, HUST. From 2008 to 2009, he was a Visiting Research Associate in the Department of Electrical and Computer Engineering at Michigan State University, East Lansing, MI, USA. In 2008, he joined HUST, where he is currently an Associate Professor. His research interests include power system operations and control and power conditioning and grid connection of alternative energy sources.